# Supporting Information for "Estimation of full moment tensors, including uncertainties, for nuclear explosions, volcanic events, and earthquakes"

**Celso Alvizuri[1,2], Vipul Silwal[1], Lion Krischer[3], Carl Tape[1]**

[1]Geophysical Institute and Department of Geosciences, University of Alaska Fairbanks, USA 99775
[2]Institute of Earth Sciences, University of Lausanne, Switzerland CH-1015
[3]Institut für Geophysik, ETH Zürich, Zürich, Switzerland CH-8092

## Contents



## References

Bennett, T. J., V. Oancea, B. W. Barker, Y.-L. Kung, M. Bahavar, B. C. Kohl, J. R. Murphy, and I. K. Bondár (2010), The Nuclear Explosion Database (NEDB): A new database and web site for accessing nuclear explosion source information and waveforms, *Seismol. Res. Lett.*, *81*(1), 12–25, doi:10.1785/gssrl.81.1.12.

Ford, S. R., D. S. Dreger, and W. R. Walter (2009), Identifying isotropic events using a regional moment tensor inversion, *J. Geophys. Res.*, *114*, B01306, doi:10.1029/2008JB005743.

Lohman, R. B., M. Simons, and B. Savage (2002), Location and mechanism of the Little Skull Mountain earthquake as constrained by satellite radar interferometry and seismic waveform modeling, *J. Geophys. Res.*, *107*(B6), doi:10.1029/2001JB000627.

Corresponding author: Celso Alvizuri, `celso.alvizuri@gmail.com`

**Table S1.** Comparison of moment tensors from this study (Figure 3b) with those of *Ford et al.* [2009] (Figure 3a). The differences are quantified in terms of the magnitude difference $\Delta M_w = M_{ford} - M_{alvizuri}$ and four angles whose allowable ranges are listed: $\omega$ is the matrix angle between moment tensors, $\omega_{dc}$ is the matrix angles between closest double couples, $\xi_0$ is the minimum angle between principal axis triples, and $\theta$ is the arc distance on the lune. If the frames are equivalent for two moment tensors, then $\omega = \theta$.

| event name | $\Delta M_w$ | $\omega$ 0–180 | $\omega_{dc}$ 0–180 | $\xi_0$ 0–120 | $\theta$ 0–180 |
|---|---|---|---|---|---|
| KERNVILLE | -0.12 | 8 | 16 | 16 | 6 |
| AMARILLO | 0.00 | 12 | 8 | 13 | 10 |
| DISKO ELM | 0.02 | 18 | 47 | 43 | 14 |
| HORNITOS | -0.12 | 10 | 36 | 43 | 4 |
| BARNWELL | -0.09 | 6 | 11 | 12 | 1 |
| METROPOLIS | 0.13 | 28 | 57 | 102 | 10 |
| BULLION | -0.01 | 9 | 37 | 36 | 1 |
| AUSTIN | -0.07 | 8 | 23 | 24 | 3 |
| HOUSTON | -0.06 | 10 | 28 | 34 | 2 |
| COSO | -0.16 | 18 | 33 | 37 | 11 |
| BEXAR | 0.06 | 17 | 30 | 40 | 10 |
| HOYA | -0.03 | 14 | 31 | 35 | 7 |
| LUBBOCK | 0.06 | 16 | 18 | 32 | 13 |
| BRISTOL | -0.06 | 14 | 9 | 17 | 12 |
| JUNCTION | -0.02 | 24 | 70 | 74 | 5 |
| HUNTERS TROPHY | -0.03 | 18 | 69 | 65 | 3 |
| DIVIDER | 0.04 | 14 | 25 | 25 | 12 |
| Little Skull Main | -0.12 | 22 | 9 | 12 | 18 |
| Little Skull Aftershock | -0.14 | 9 | 3 | 5 | 8 |
| Timber Mountain | -0.00 | 25 | 20 | 20 | 18 |
| Amargosa | -0.12 | 45 | 11 | 12 | 44 |
| Groom Pass | 0.08 | 29 | 32 | 31 | 26 |
| Indian Springs | 0.07 | 30 | 20 | 21 | 21 |
| Calico Fan | -0.09 | 26 | 21 | 21 | 20 |
| Warm Springs | -0.00 | 61 | 56 | 57 | 13 |
| Frenchman Flat 1 | 0.01 | 48 | 13 | 14 | 46 |
| Frenchman Flat 2 | -0.06 | 20 | 29 | 31 | 11 |
| Little Skull | -0.19 | 27 | 16 | 20 | 19 |
| Ralston | -0.03 | 15 | 8 | 10 | 10 |
| ATRISCO Hole | -0.17 | 24 | 52 | 66 | 9 |
| Trona Mine 1 | -0.28 | 39 | 94 | 79 | 18 |
| Trona Mine 2 | -0.03 | 13 | 22 | 34 | 3 |

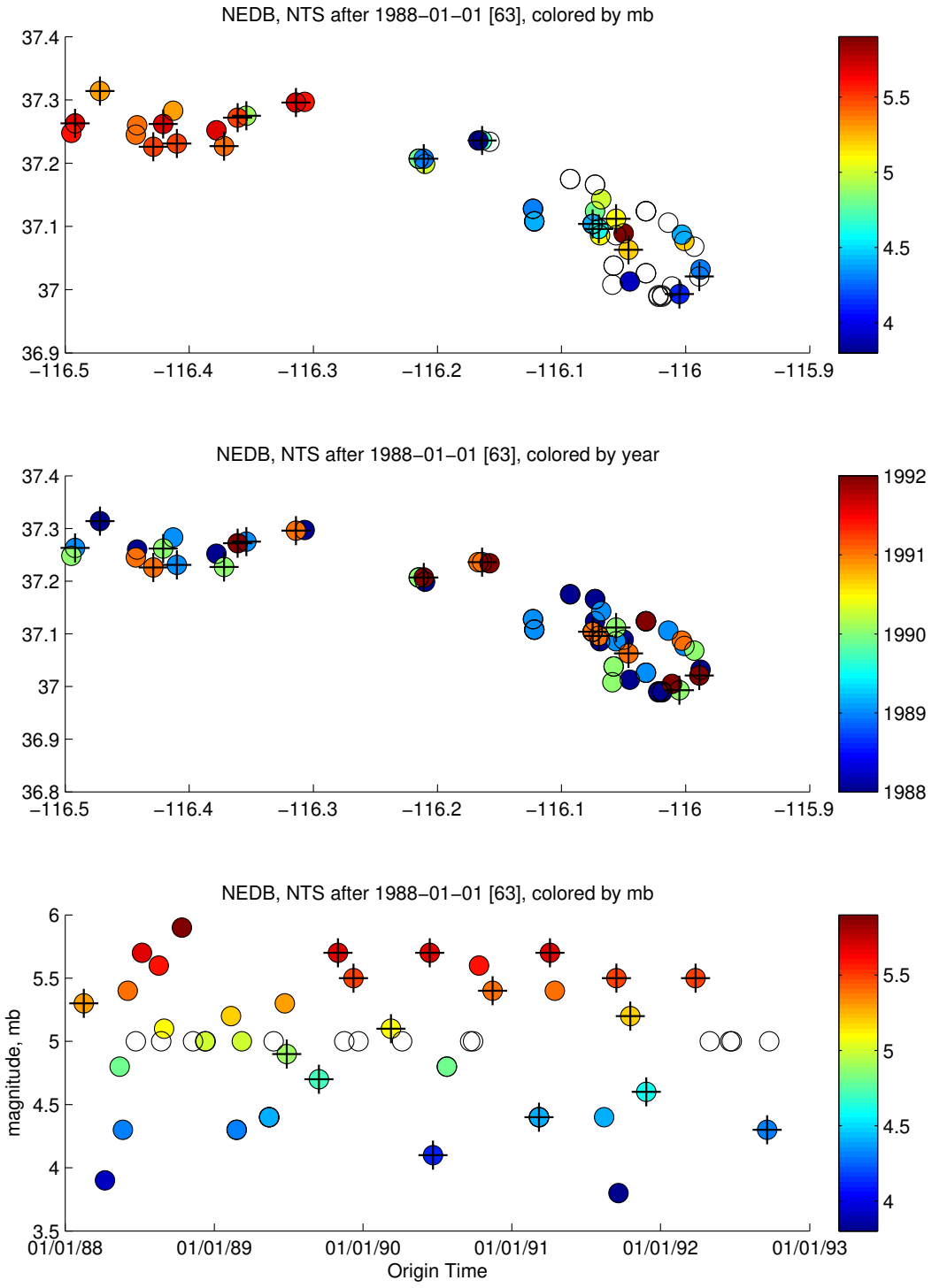


**Figure S1.** All events since 1988-01-01 within the Nevada Test Site; data from the Nuclear Explosion Database [*Bennett et al.*, 2010]. The cross symbols denote the 17 events from *Ford et al.* [2009]. The top two subplots show the 63 events in map view, colored by magnitude $m_b$ (top) or year (middle). The bottom subplot shows $m_b$ vs time, colored by magnitude. Events without an $m_b$ are plotted as open circles with a value of 5.

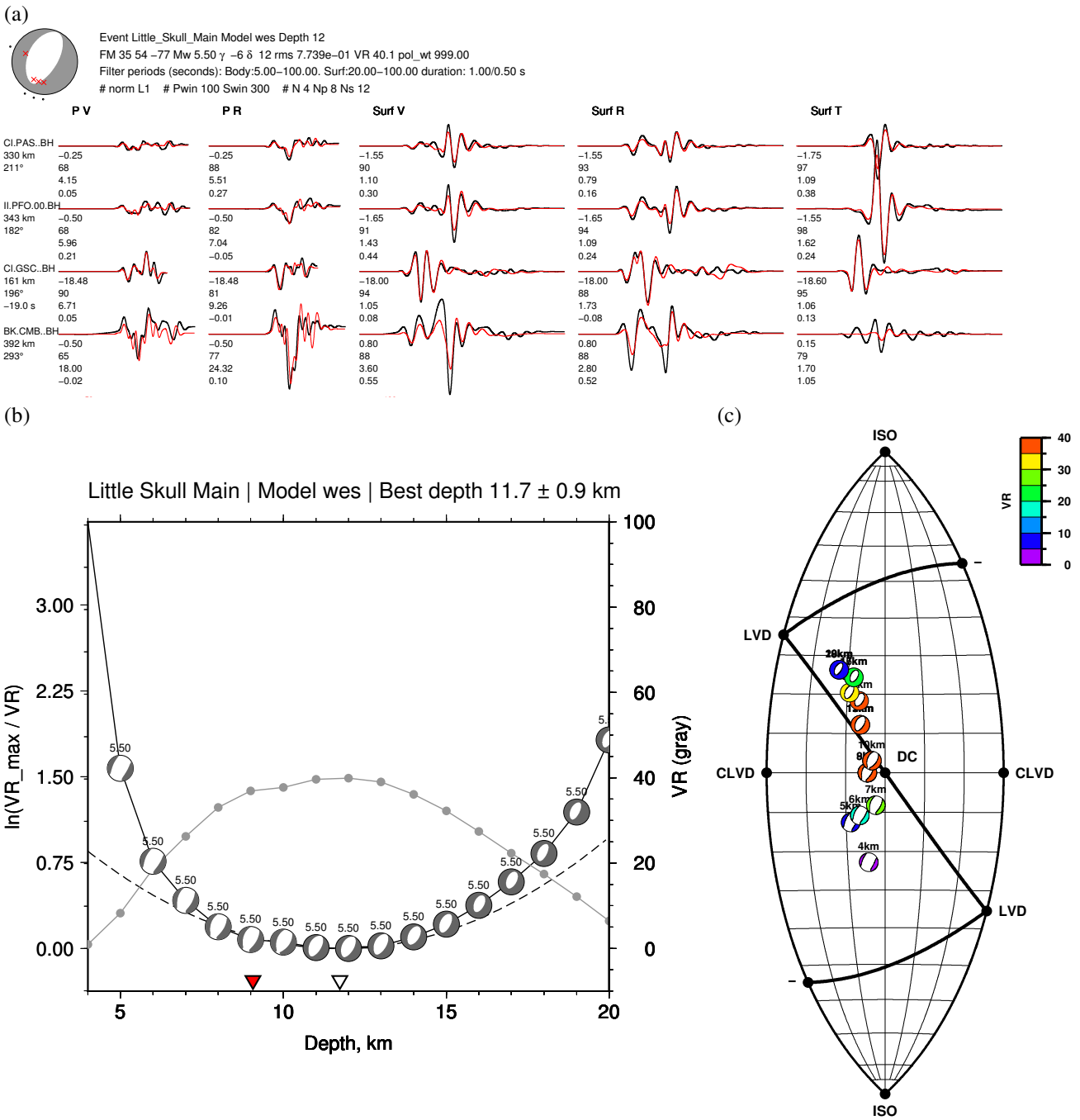


**Figure S2.** Validation test using the stations and bandpass of *Lohman et al.* [2002] for the Little Skull Mountain earthquake: 5–100 s for body waves and 20–100 s for surface waves. (a) Waveform fits for the best-fitting moment tensor; the depth of 12 km is the (rounded) depth of 12 km from Table 1 of *Lohman et al.* [2002]. (b) Grid search over depth. The best-fitting depth is 11.7 km (white arrow), and the catalog depth (red arrow) is 9 km (Table 2). (c) Lune plot version of (b), showing the variation in moment tensor source type (and *VR*) as the depth changes. For this example, the isotropic component (i.e., lune latitude) is negative at shallowest depths and positive at deepest depths.

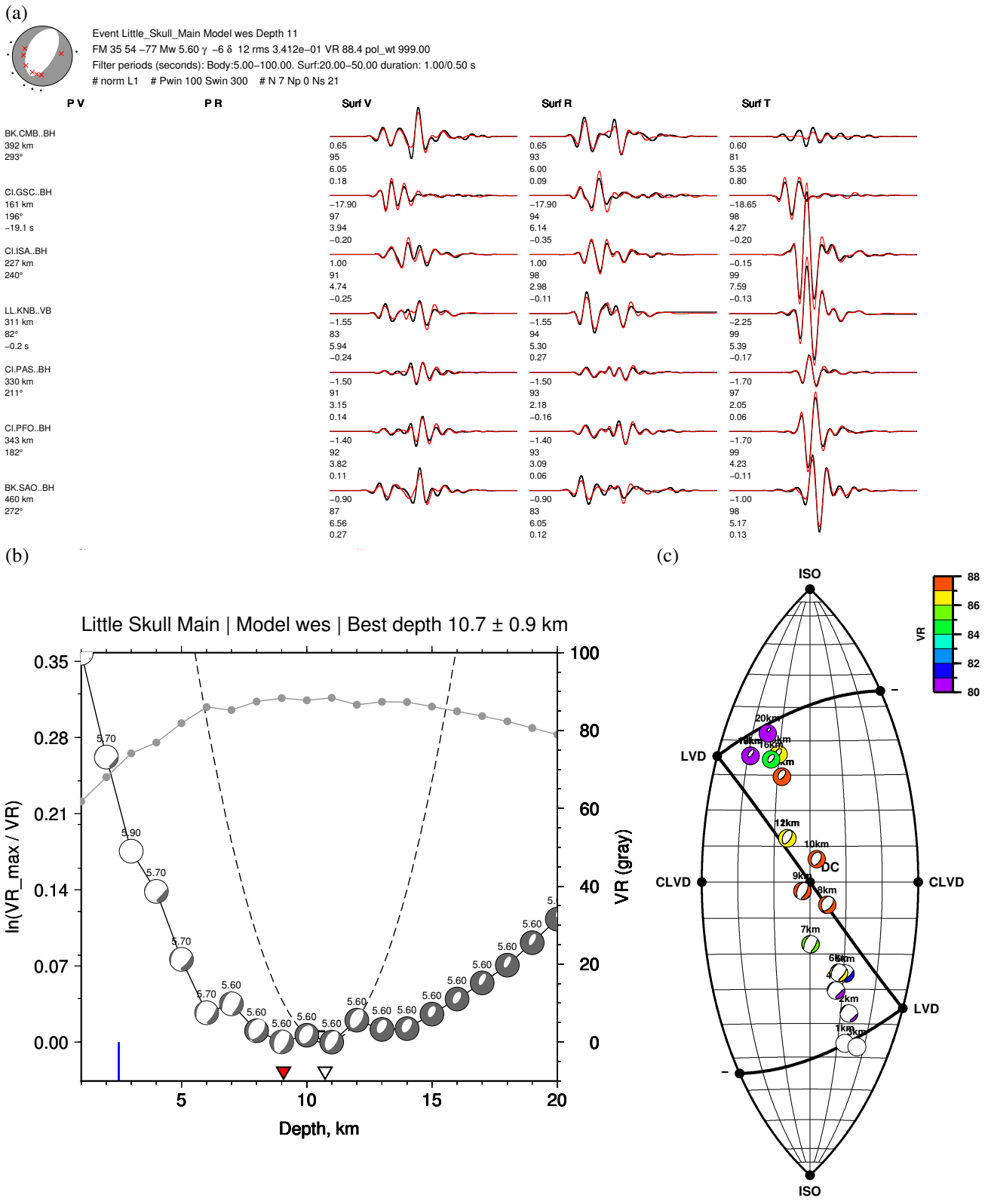


**Figure S3.** Validation test using the stations and bandpass of *Ford et al.* [2009] for the Little Skull Mountain earthquake: 20–50 s for surface waves. (a) Waveform fits for the best-fitting moment tensor; the depth of 11 km is based on the results in (b). The best-fitting magnitude is $M_w$ 5.6. Our waveform fits for this event are shown in Figure S4. (b) Grid search over depth. The best-fitting depth is 10.7 km (white arrow), and the catalog depth (red arrow) is 9 km (Table 2). (c) Lune plot version of (b), showing the variation in moment tensor source type (and *VR*) as the depth changes. For this example, the isotropic component (i.e., lune latitude) is negative at shallowest depths and positive at deepest depths.

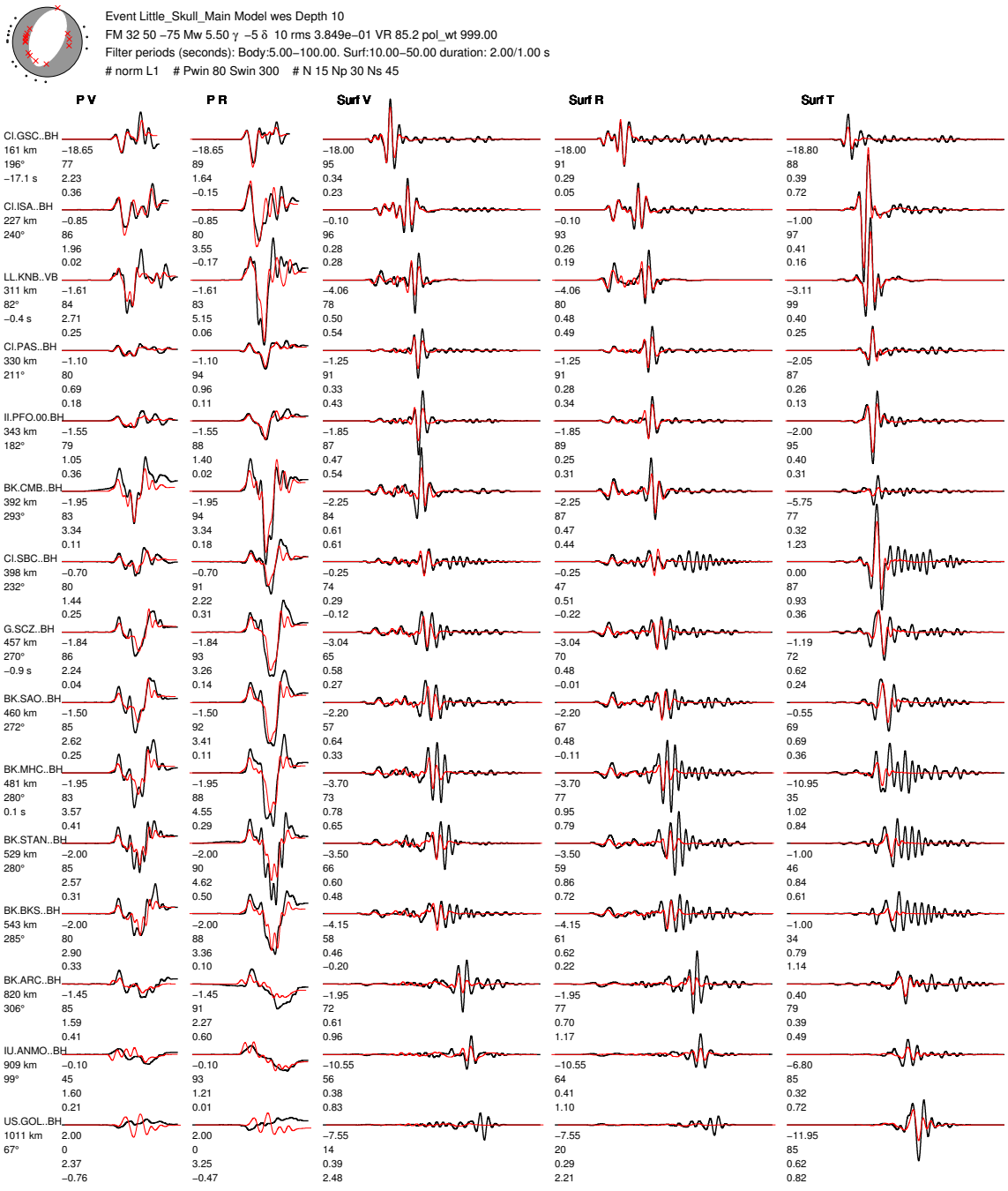


**Figure S4.** Our best-fitting moment tensor for the Little Skull Mountain earthquake. The body-wave bandpass is 5–100 s, and the surface-wave bandpass is 10–50 s. The depth of 10 km is based on the depth search in Figure S10a.

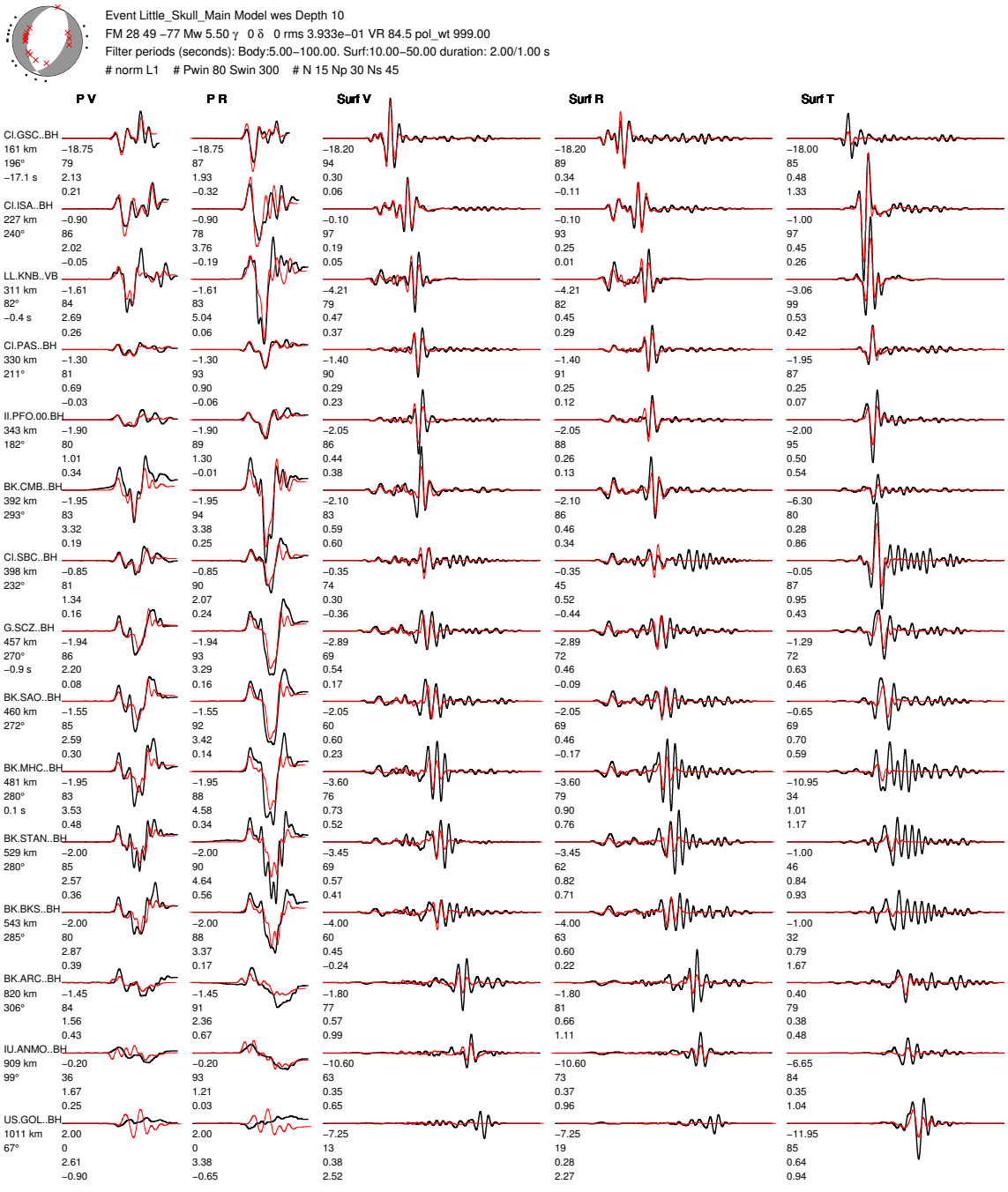


**Figure S5.** Same as Figure S4 but for the best-fitting double-couple moment tensor.

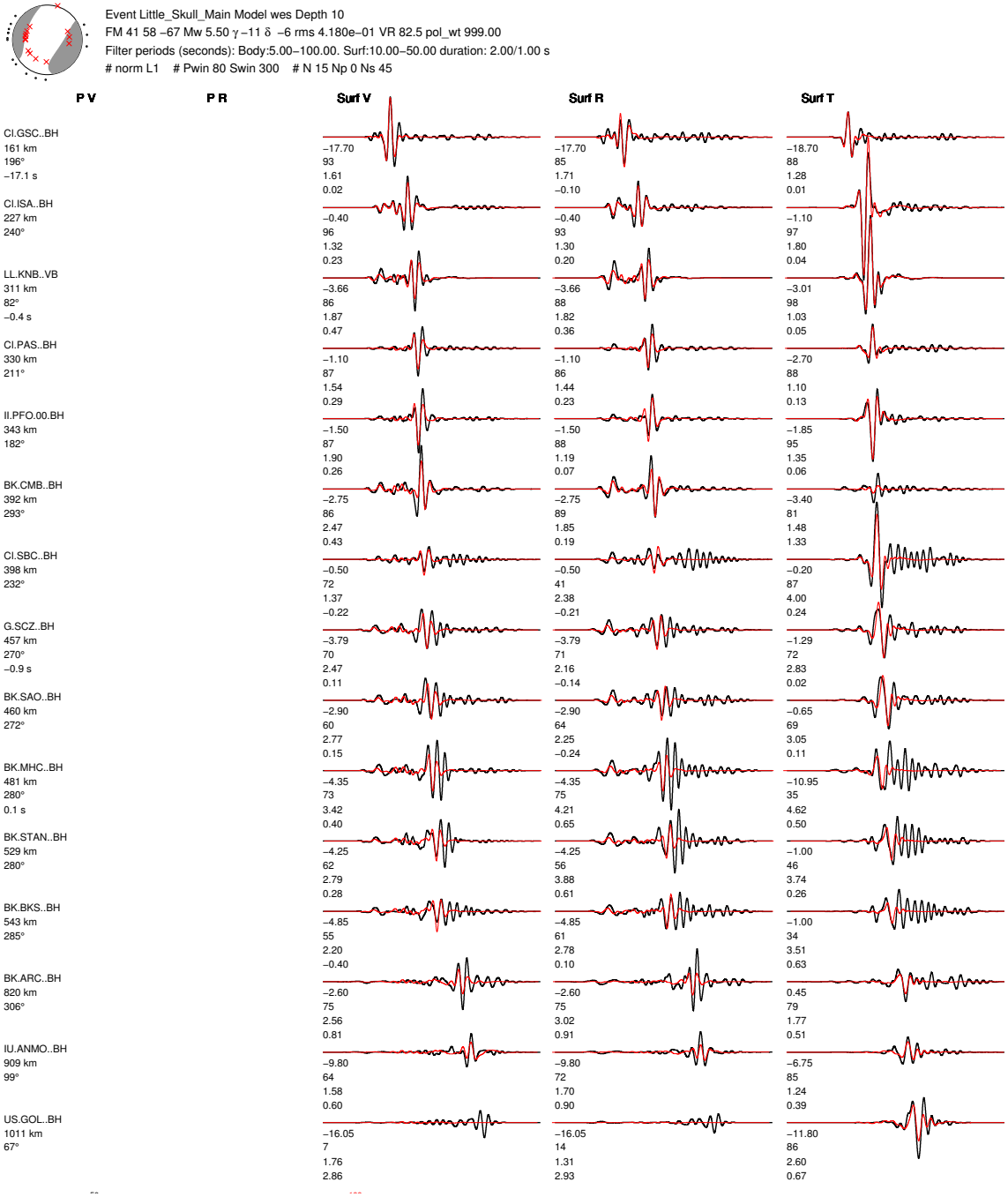


**Figure S6.** Best-fitting moment tensor and corresponding waveform fits for the Little Skull Mountain, bandpass periods 10–50 s, surface waves only. Shorter periods are included in Figures S7 and S8.

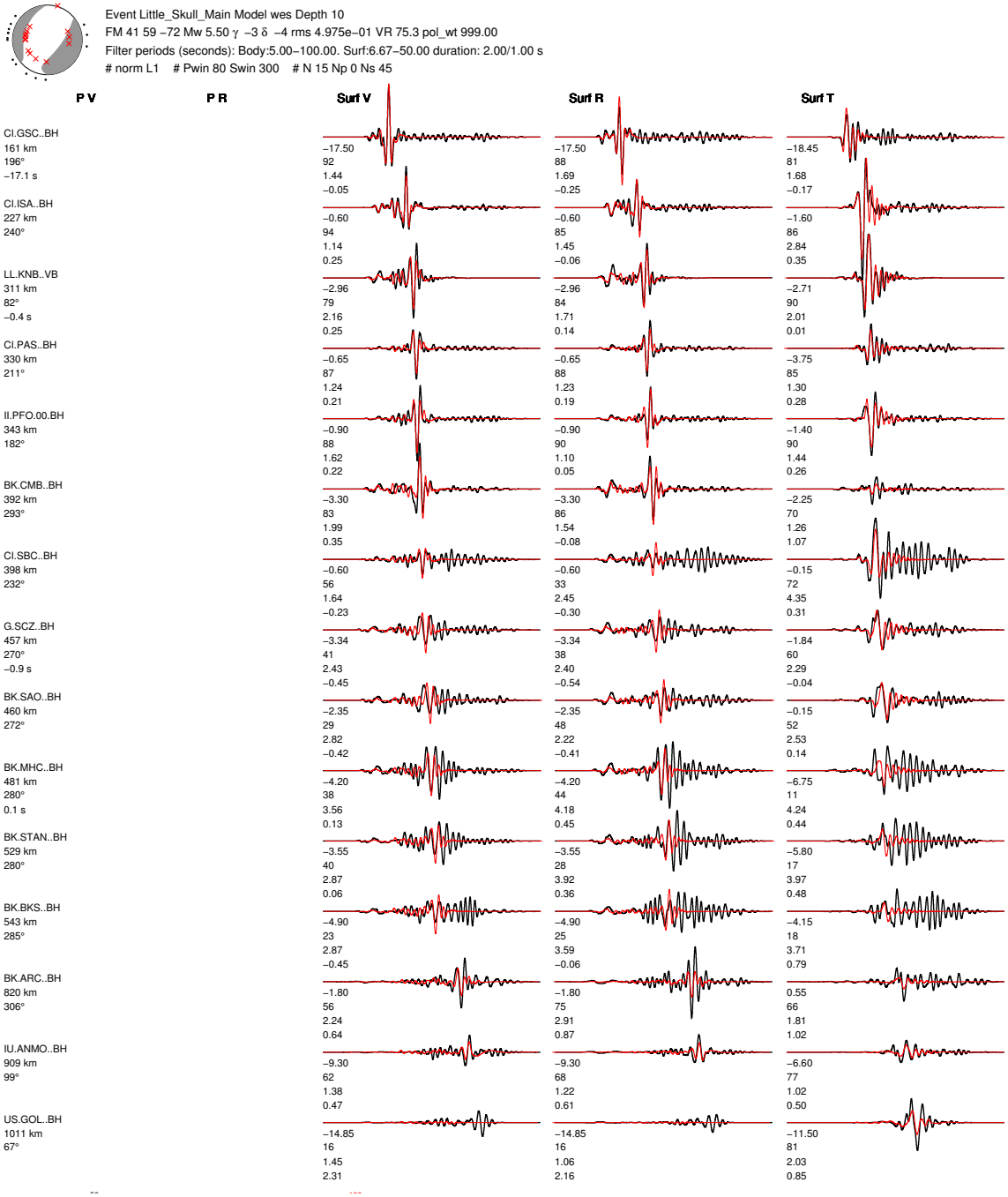


**Figure S7.** Best-fitting moment tensor and corresponding waveform fits for the Little Skull Mountain, bandpass periods 7–50 s, surface waves only.

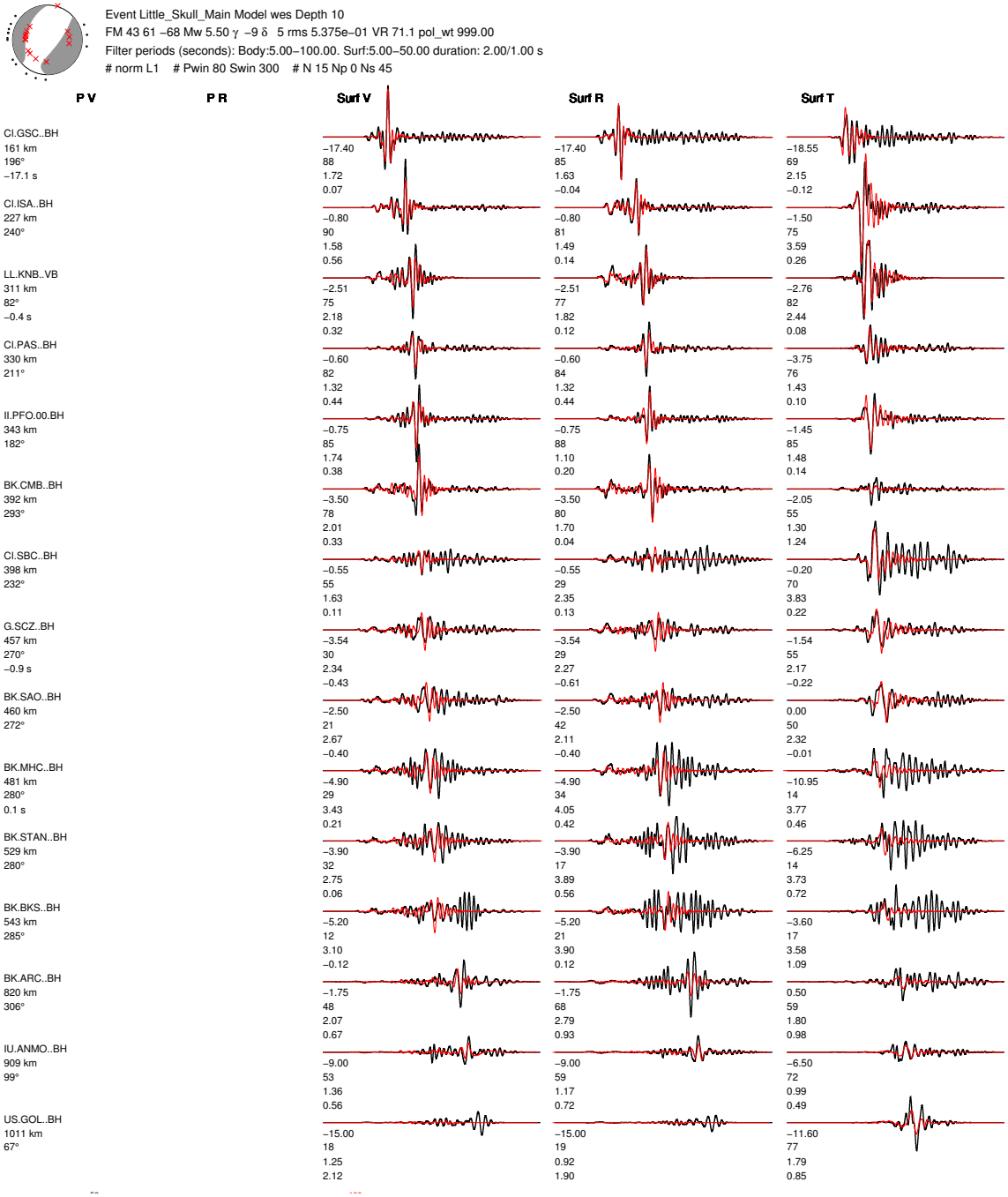


**Figure S8.** Best-fitting moment tensor and corresponding wveform fits for the Little Skull Mountain, bandpass periods 5–50 s, surface waves only.

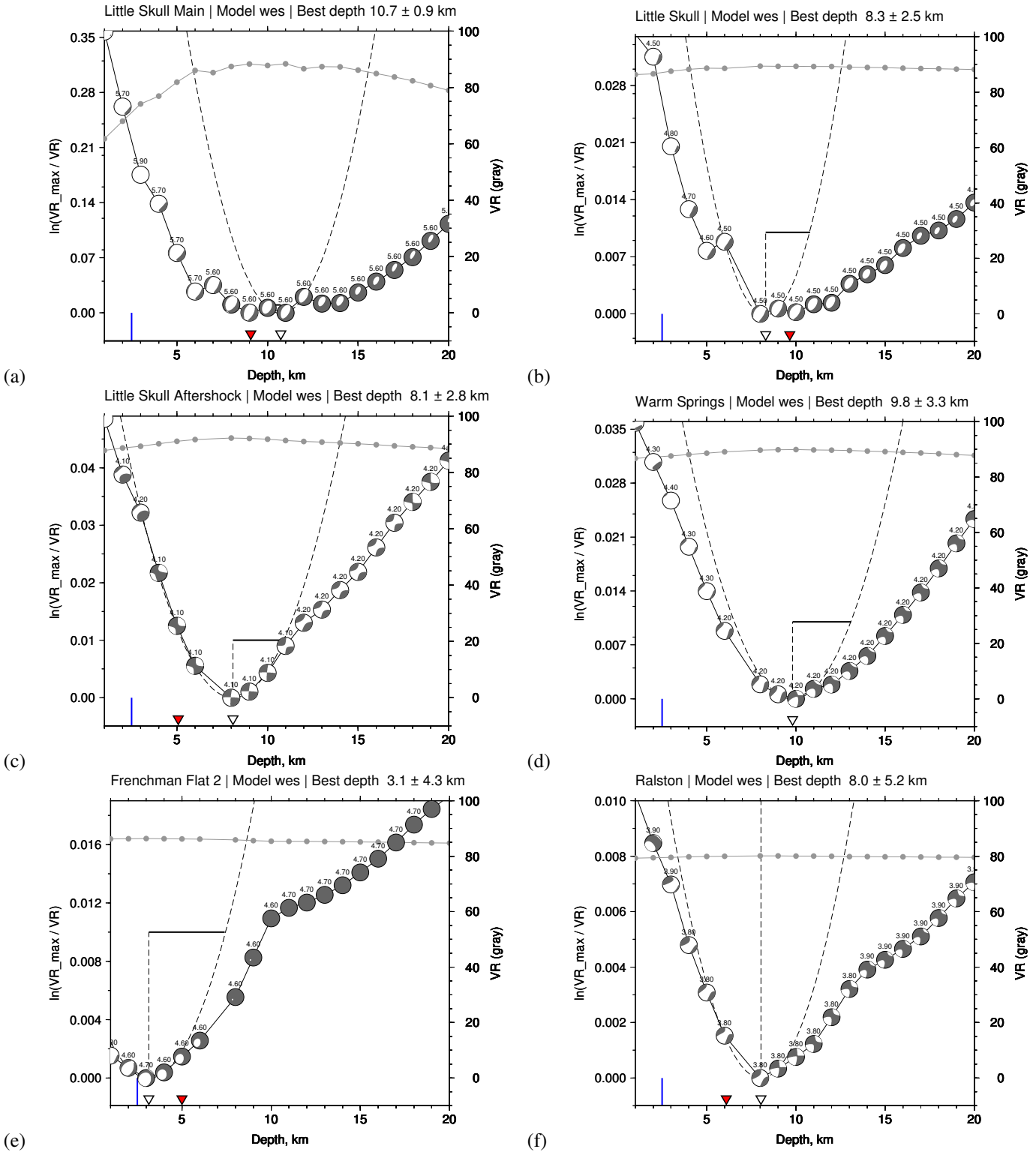


**Figure S9.** Grid search over depth for NTS earthquakes 1–6 using the bandpass limit 20–50 s. For each depth, a search over all moment tensors (including magnitude) is performed.

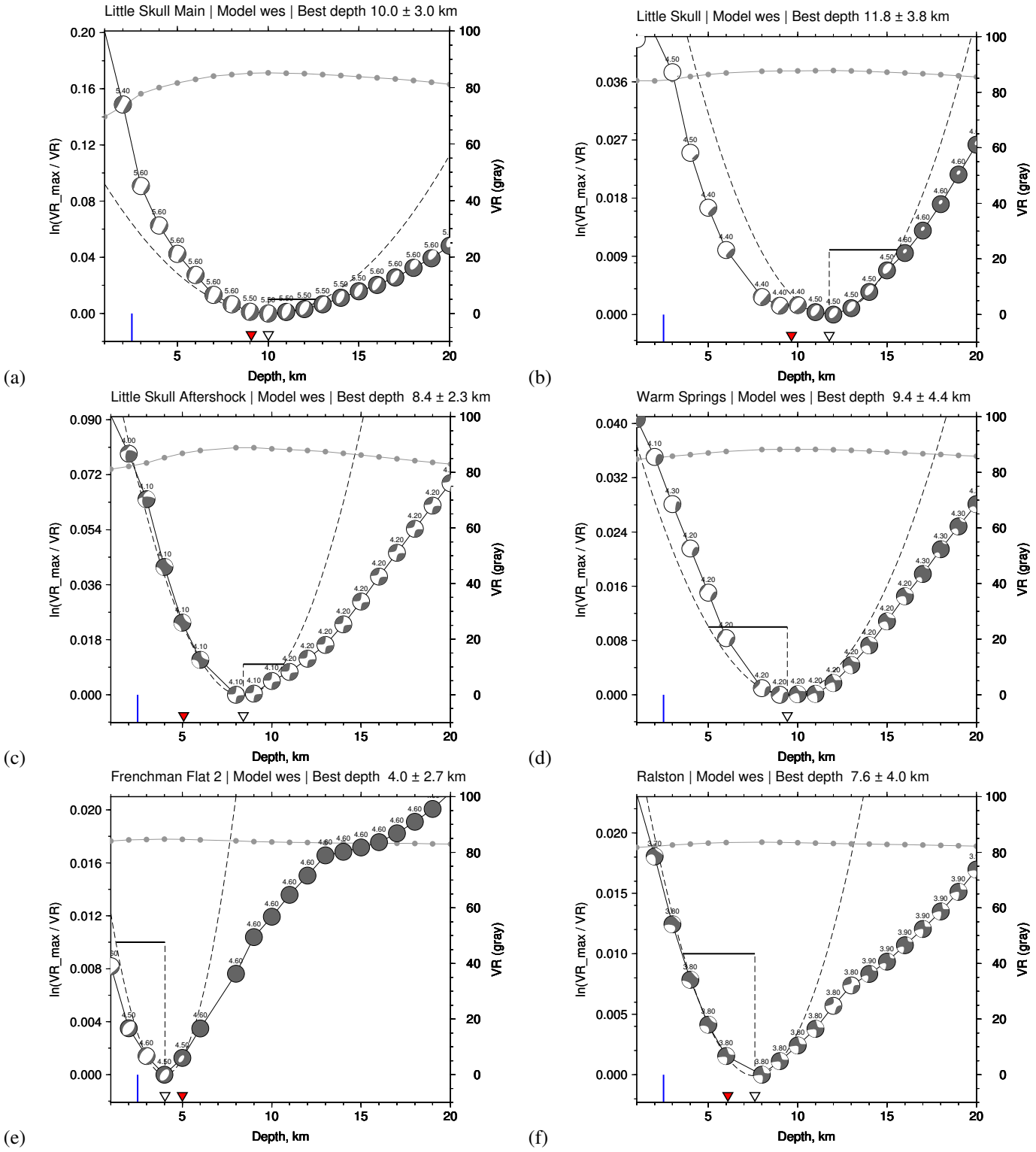


**Figure S10.** Grid search over depth for NTS earthquakes 1–6 using the bandpass limits listed in Table 3. For each depth, a search over all moment tensors (including magnitude) is performed.

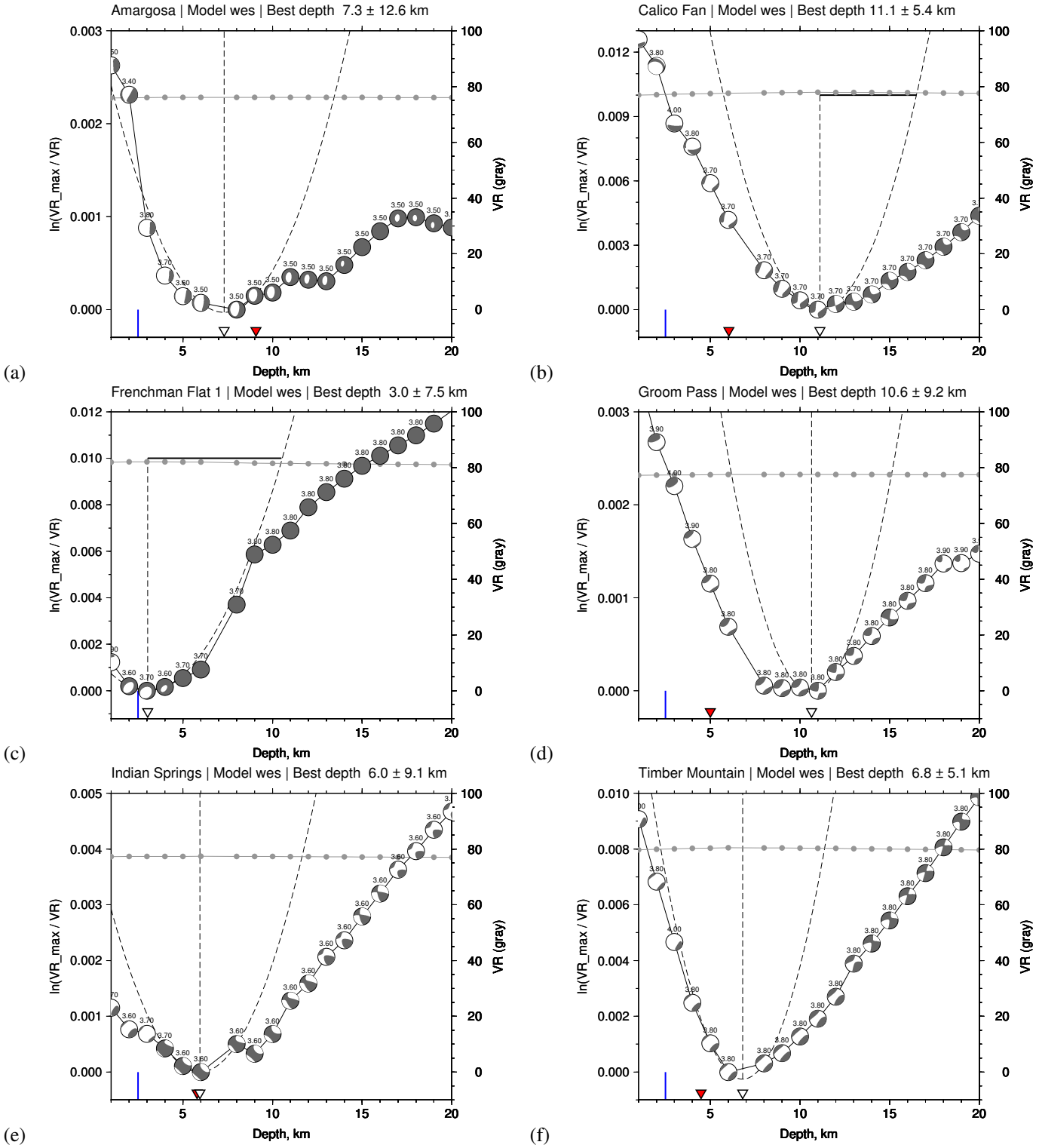


**Figure S11.** Grid search over depth for NTS earthquakes 7–12 using the bandpass limit 20–50 s. For each depth, a search over all moment tensors (including magnitude) is performed.

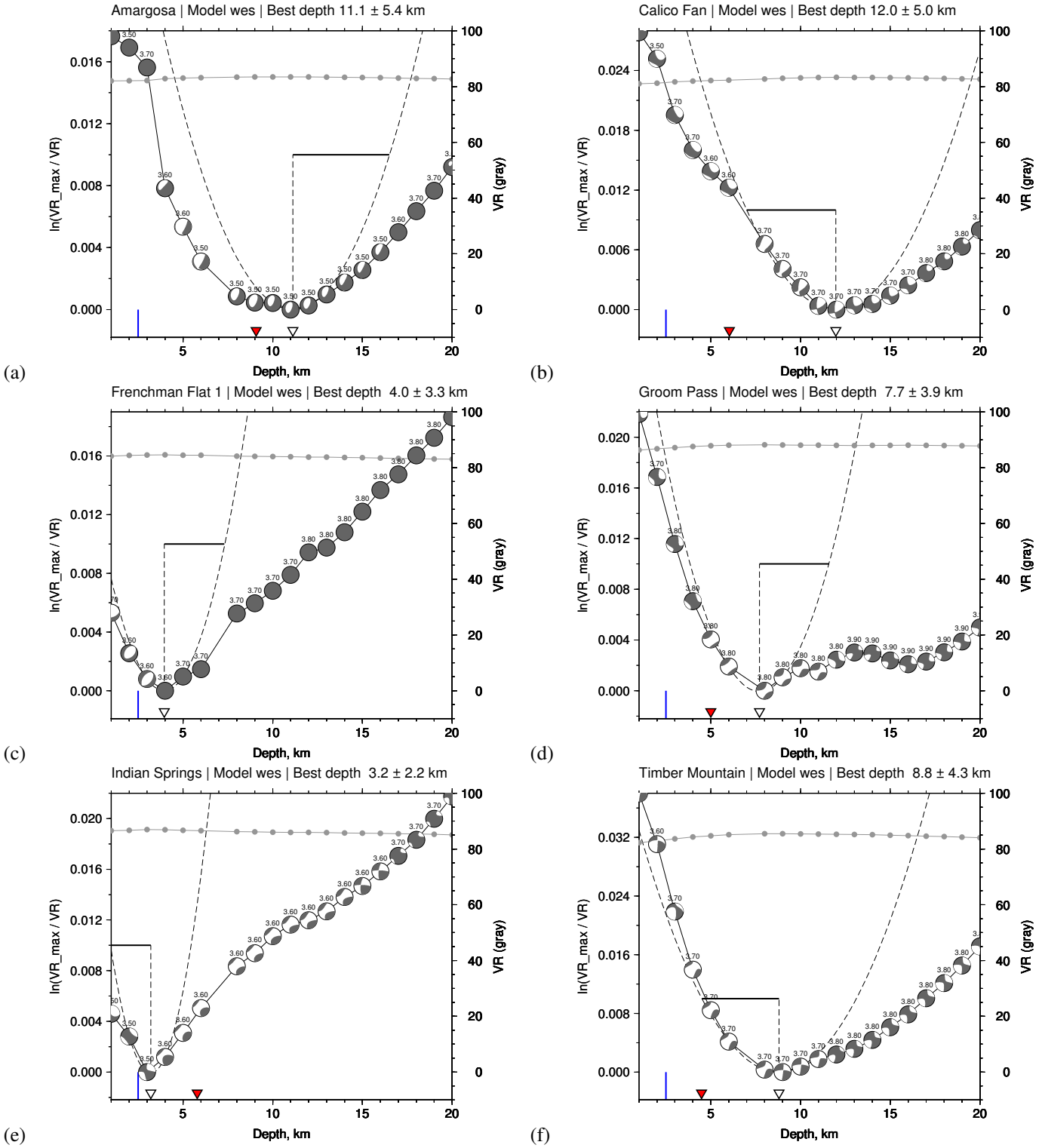


**Figure S12.** Grid search over depth for NTS earthquakes 7–12 using the bandpass limits listed in Table 3. For each depth, a search over all moment tensors (including magnitude) is performed.

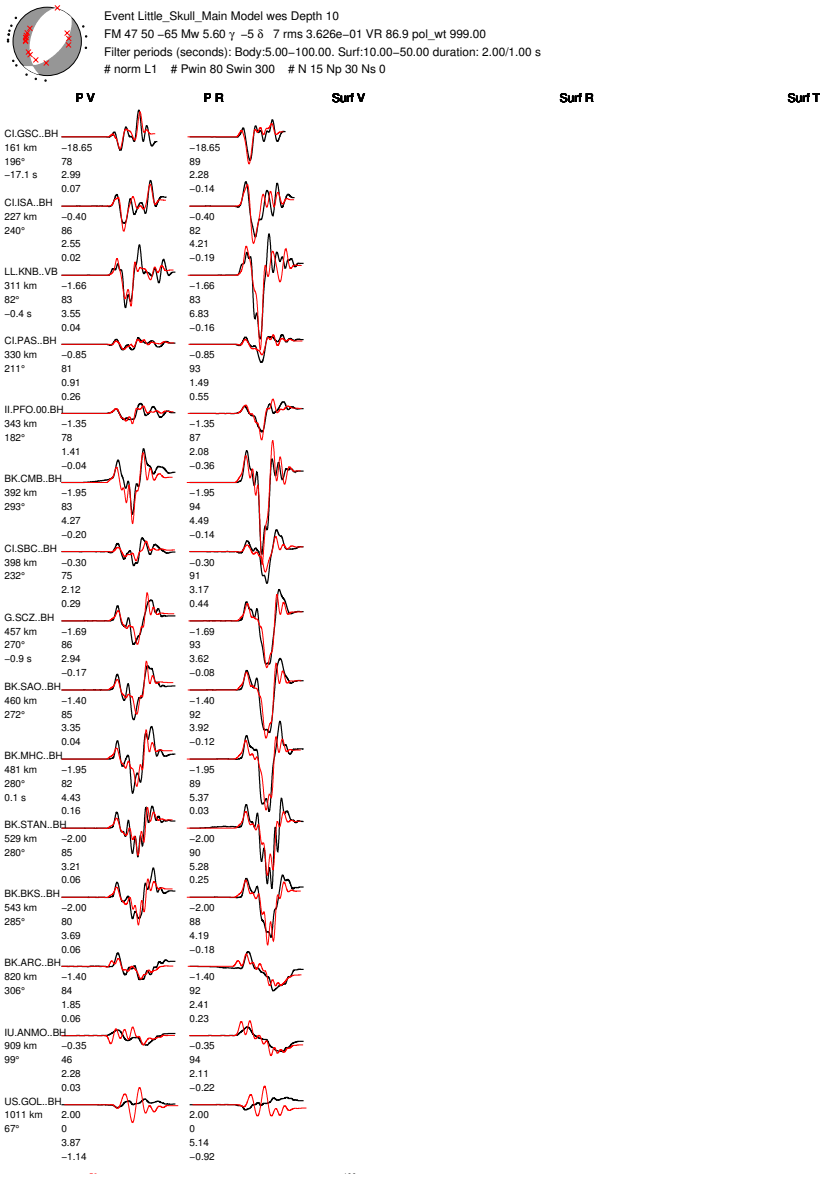


**Figure S13.** Best-fitting moment tensor and corresponding waveform fits for the Little Skull Mountain earthquake using body waves only (5–100 s). See lune plot in Figure 10a. Waveform fits for the combined body wave and surface wave inversion are shown in Figure S4.

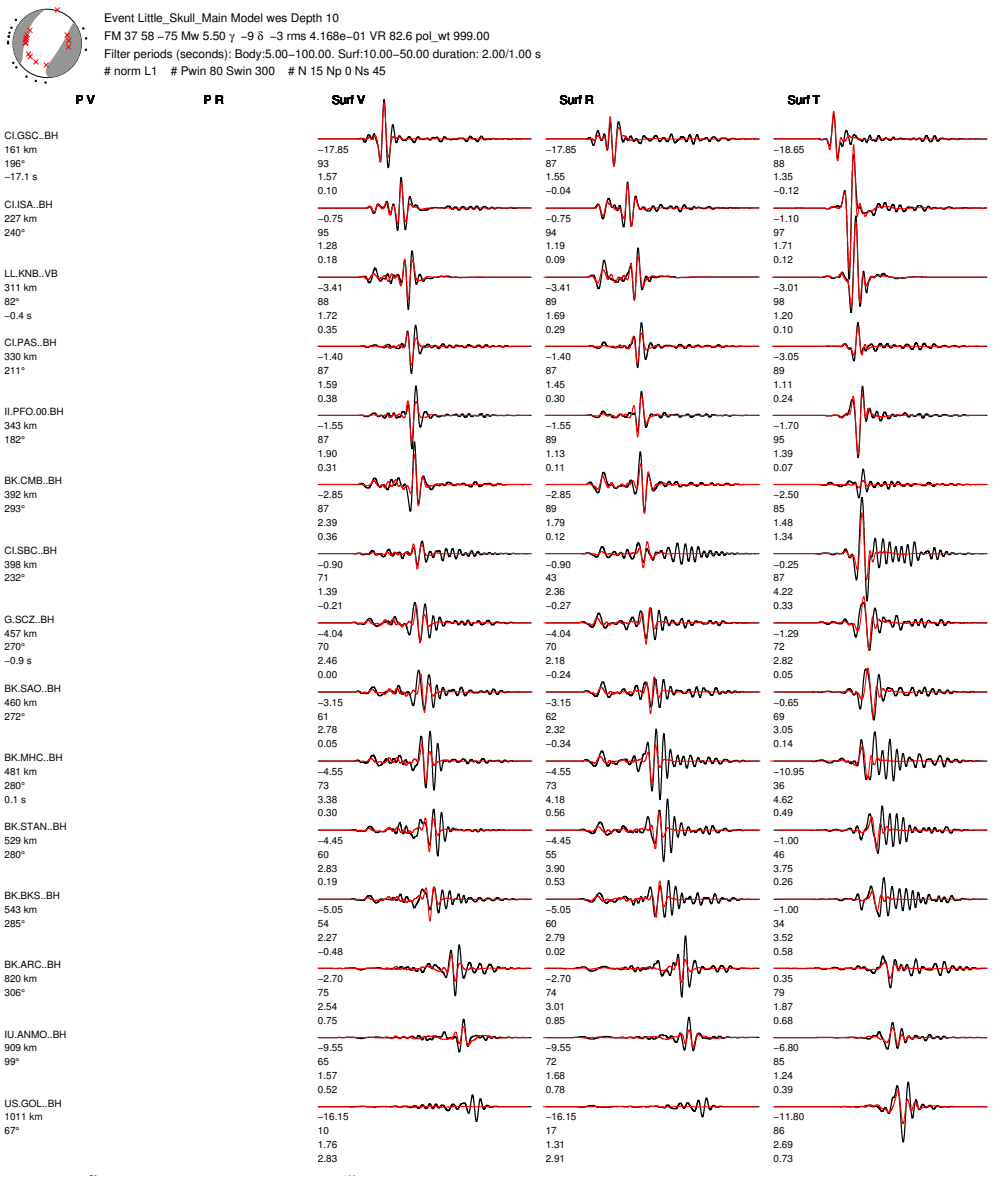


**Figure S14.** Best-fitting moment tensor and corresponding waveform fits for the Little Skull Mountain earthquake using surface waves only (10–100 s). See lune plot in Figure 10b. Waveform fits for the combined body wave and surface wave inversion are shown in Figure S4.

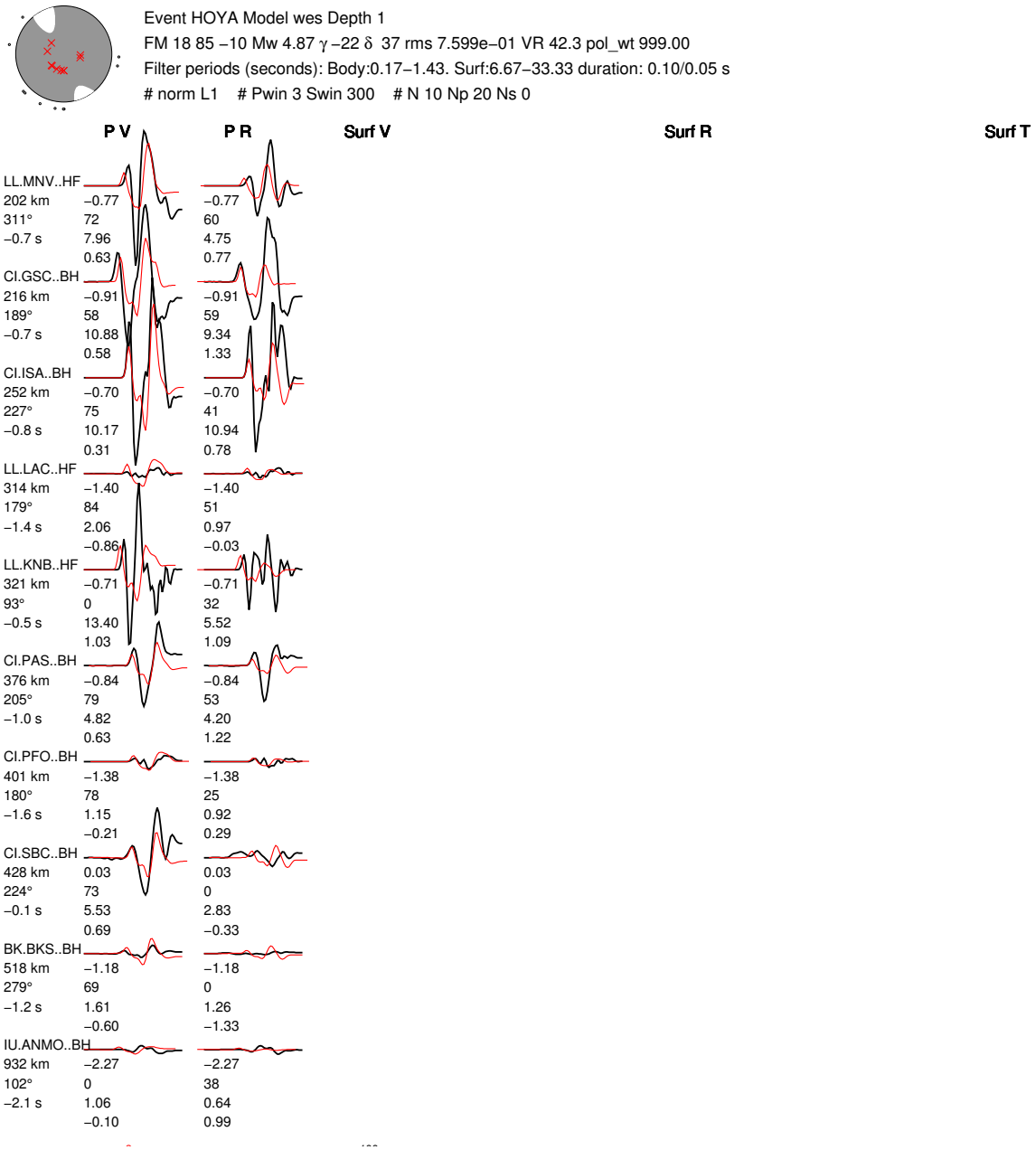


**Figure S15.** Best-fitting moment tensor and corresponding waveform fits for the HOYA nuclear explosion using body waves only (0.7–6.0 Hz). See lune plot in Figure 10d.

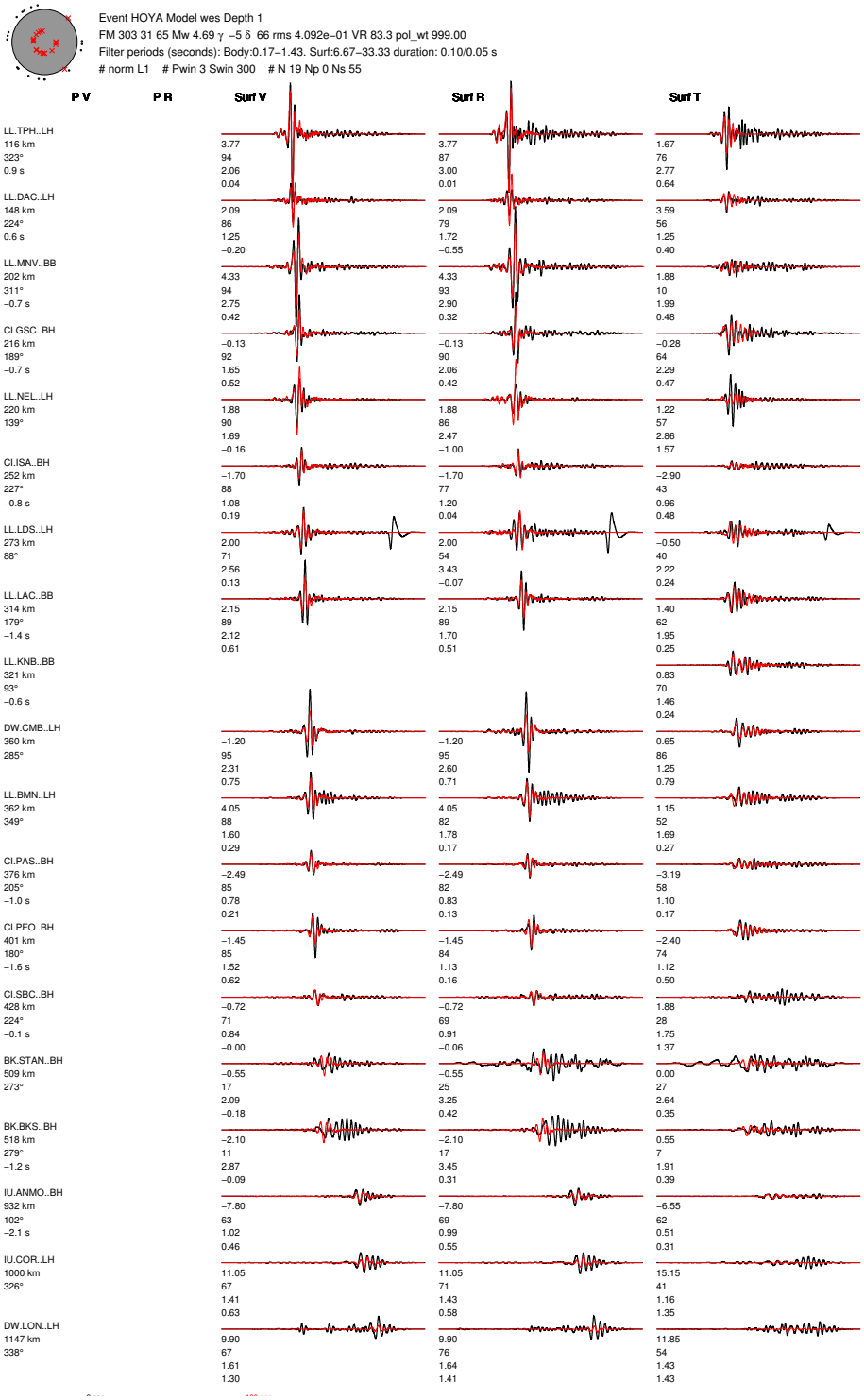


**Figure S16.** Expanded version of Figure 4. Best-fitting moment tensor and corresponding waveform fits for the HOYA nuclear explosion using surface waves only (7–33 s). See lune plot in Figure 10e.

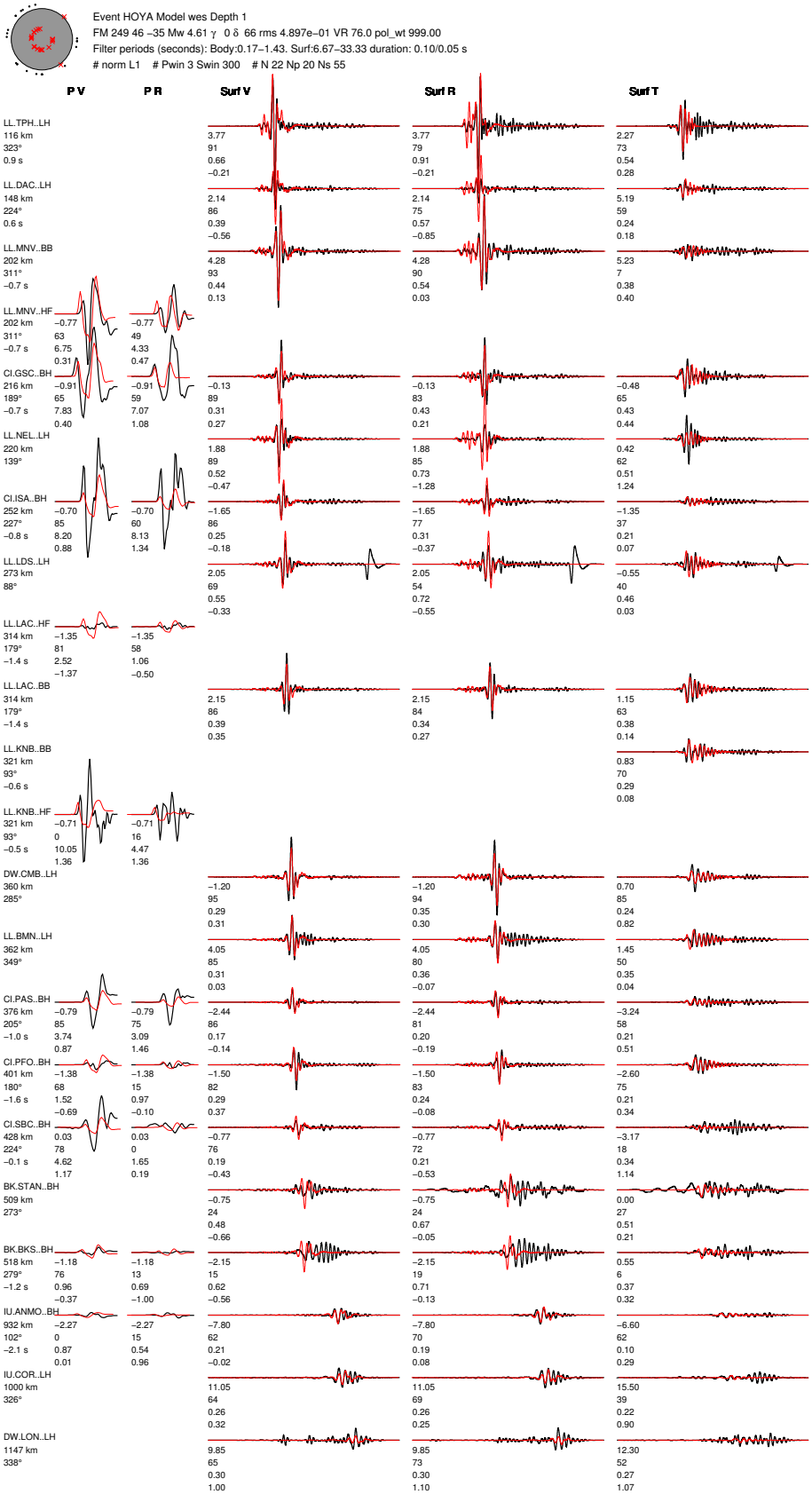


**Figure S17.** Best-fitting moment tensor and corresponding waveform fits for the HOYA nuclear explosion using body waves (0.7–6.0 Hz) and surface waves (7–33 s). See lune plot in Figure 10f.